

# Electron-spin resonance of $\text{Eu}^{+2}$ spins in metallic $\text{EuCo}_{2-y}\text{As}_2$ single crystals

N. S. Sangeetha,<sup>1</sup> S. D. Cady,<sup>2</sup> and D. C. Johnston<sup>1,3</sup>

<sup>1</sup>*Ames Laboratory, Iowa State University, Ames, Iowa 50011, USA*

<sup>2</sup>*Chemical Instrumentation Facility, Iowa State University, Ames, Iowa 50011, USA*

<sup>3</sup>*Department of Physics and Astronomy, Iowa State University, Ames, Iowa 50011, USA*

(Dated: October 21, 2019)

The body-centered-tetragonal metallic compound  $\text{EuCo}_{2-y}\text{As}_2$  orders into an antiferromagnetic helical structure below a temperature  $T_N = 40\text{--}45$  K, where the effective moment of the Eu spins-7/2 in the paramagnetic state is enhanced by about 7% above the value expected for spectroscopic splitting factor  $g = 2$ , and the saturation moment at high fields and low  $T$  is also sometimes enhanced compared to the value for  $g = 2$ . Here we report X-band electron-spin resonance (ESR) measurements of the microscopic magnetic behavior of the Eu spins that were carried out to identify the origin of these enhanced moments. We infer that the enhancements arise from ferromagnetic polarization of the Co 3d band electrons by the Eu spins, where the polarized band electrons form a spin cloud around the Eu spins that adiabatically follows the motion of the Eu spins. In the past, the theoretically-required magnetic-field  $H$  prefactor to the expression for the field-dependent microwave ESR power absorption was omitted from fits of the ESR spectra for high concentrations of local magnetic moments in metals. Here we fitted the ESR spectra for  $\text{EuCo}_{2-y}\text{As}_2$  both with and without the  $H$  prefactor in the fitting expression and found that the Dysonian  $\alpha$  parameter is strongly affected when the  $H$  prefactor is omitted, whereas the resonant field and linewidth are changed by only a few percent. The integrated power absorption between  $H = 0$  and  $H = \infty$  is finite if the  $H$  prefactor is ignored, whereas it diverges if the prefactor is included as discussed in the Appendix.

## I. INTRODUCTION

The  $S$ -state ions  $\text{Eu}^{+2}$  and  $\text{Gd}^{+3}$  have the electronic configuration  $4f^7$  with spin  $S = 7/2$  and orbital angular momentum  $L = 0$ . Therefore spin-orbit coupling of these ions is very weak and their spectroscopic splitting factors ( $g$ -factors) are both close to the free-electron value of 2. The effective moment for  $g = 2$  and  $S = 7/2$  is  $\mu_{\text{eff}} = g\sqrt{S(S+1)}\mu_B = 7.94\ \mu_B$ , where  $\mu_B$  is the Bohr magneton. In most compounds containing these ions, magnetic susceptibility ( $\chi$ ) measurements in the paramagnetic state reveal  $\mu_{\text{eff}}$  values close to this value. For example, for the  $\text{Eu}^{+2}$  spins in the paramagnetic state of the helical antiferromagnet  $\text{EuCo}_2\text{P}_2$  with the body-centered tetragonal  $\text{ThCr}_2\text{Si}_2$  structure,  $\mu_{\text{eff}}$  is equal to the predicted value and the ordered (saturation) moment at low temperatures is also equal to the predicted value  $\mu_{\text{sat}} = gS\mu_B = 7.0\ \mu_B/\text{Eu atom}$  [1].

However, in the isostructural compound  $\text{EuCo}_2\text{As}_2$ ,  $\mu_{\text{eff}}$  was found to be about  $8.5\ \mu_B/\text{Eu atom}$ , corresponding to a 7.1% enhancement of the  $g$  value [2]. From electronic structure calculations, this enhancement was found to be due to ferromagnetic polarization of the Co 3d electrons by the Eu spins [2]. One can envision two scenarios for the implementation of this polarization. In one scenario, the enhancement could come from polarization of nearly localized 3d electrons around the Co atoms and in the second one, the enhancement could originate from polarization of itinerant Co 3d band electrons in the vicinity of the Eu spins. In the latter case, one would expect microscopic measurements of the Eu  $g$ -factor to show an enhancement of about 7%, whereas in the former case not so much. The present Eu electron-spin resonance

(ESR) measurements were carried out in the paramagnetic state from 50 K to 180 K to obtain a microscopic measurement of the degree to which the Eu  $g$ -factor is enhanced, if at all. We found that the  $g$ -factor of the Eu spins is strongly temperature  $T$  dependent, and that the  $g$ -factor averaged over temperature is enhanced above the free-electron value  $g = 2$  for the two Crystals #2 and #3 that we measured by 5% and 7.1%, respectively. We infer that the enhanced  $g$ -factor as reflected by the enhanced effective moment in the magnetic susceptibility experiments arises from a ferromagnetically-polarized conduction-electron spin cloud around each Eu spin.

Because  $\text{EuCo}_{2-y}\text{As}_2$  is metallic, in the present work we expected and found a Dysonian lineshape of the Eu ESR versus applied field  $H$ . The theoretically-predicted  $H$  prefactor in the expression for the microwave power absorption by local magnetic moments in metals has always been ignored in the past to our knowledge when fitting Dysonian ESR lineshapes for high-concentrations of local magnetic moments. We recently showed [3] that including this prefactor has a significant influence on the measured field-derivative lineshape ( $A/B$  ratio) and amplitude of the microwave power absorption. Therefore, in the present work we quantitatively tested the influence of this prefactor on the fitted values of the lineshape parameters, which are the resonant field  $H_{\text{res}}$ , the Lorentzian half-width at half maximum peak height  $\Delta H$ , and the Dysonian parameter  $\alpha$  which is the ratio of the dispersive to the absorptive magnetic susceptibilities that are present in the Dysonian absorptive susceptibility  $\chi''_{\text{D}}(H)$ . We find that the fitted  $\alpha$  parameter is strongly increased by up to a factor of  $\sim 3$  when the  $H$  prefactor in  $\chi''_{\text{D}}(H)$  is ignored compared to that obtained when the prefac-

tor is present, whereas  $H_{\text{res}}$  and  $\Delta H$  are only weakly affected when the  $H$  prefactor is absent. Furthermore, without this  $H$  prefactor, the double integral of the field-derivative microwave power absorption spectrum versus field  $H$  from  $H = 0$  to  $\infty$  gives a finite result and has frequently been used to obtain a value proportional to the dc  $\chi$  in the paramagnetic state. However, when the  $H$  prefactor is included as dictated by theory, the double integral is logarithmically divergent versus  $H$  [3] and such calculations are problematic.

In Sec. II the experimental details are given, followed by presentation of the results of the ESR measurements and analyses in Sec. III. An overview of the obtained ESR field-derivative spectra is first presented, followed by the results and analyses of the fitted values of  $\alpha$ ,  $H_{\text{res}}$ ,  $g$ -factor, and  $\Delta H$ . A summary is given in Sec. IV. In the Appendix the integrated power absorption  $P_{\text{int}}$  from  $H = 0$  to a maximum field  $H^{\text{max}}$  is discussed, where  $P_{\text{int}}(H^{\text{max}} \rightarrow \infty)$  is finite if the above-noted  $H$  prefactor is ignored, whereas  $P_{\text{int}}(H^{\text{max}} \rightarrow \infty)$  diverges if the theoretically-required  $H$  prefactor is present.

## II. EXPERIMENTAL DETAILS

Two single crystals of  $\text{EuCo}_{2-y}\text{As}_2$  labeled Crystals #2 and #3 were studied that were taken from the same batches of crystals from which extensive crystallographic and physical-property data for crystals also labeled Crystals #2 (Sn-flux-grown) and #3 (CoAs self-flux-grown) were presented in Ref. [2]. The CW ESR measurements were carried out at an X-band frequency of 9.380 GHz and magnetic field scan range 0–6 kOe using an Elexsys E580 FT/CW EPR spectrometer in CW mode. The static magnetic field  $\mathbf{H}$  was applied along the  $c$  axis of the two crystals measured. The microwave magnetic field was perpendicular to  $\mathbf{H}$  and hence directed along the two large flat surfaces of the crystals parallel to the  $ab$ -plane. The ESR data reported here cover the temperature  $T$  range from 50 K to 180 K which is in the paramagnetic temperature region of the two crystals above their respective Néel temperatures of 45 K for Crystal #2 and 40 K for Crystal #3 [2]. To improve the signal-to-noise ratio, the applied magnetic field was modulated at a frequency of 100 kHz with lock-in amplifier detection at that frequency, so a measured ESR spectrum is the field derivative of the microwave power absorption spectrum.

## III. RESULTS AND ANALYSES

### A. ESR Spectra Overview

The field-derivative spectra for each of the two crystals #2 and #3 of  $\text{EuCo}_{2-y}\text{As}_2$ , at  $T = 50$  K and 180 K, are shown in Fig. 1 and exhibit Dysonian lineshapes. The Dysonian absorptive susceptibility  $\chi''_{\text{D}}(H)$  including

both the rotating and counter-rotating components of the linearly-polarized microwave field  $\mathbf{H}_1$  applied perpendicular to the applied field direction is [3–5]

$$\chi''_{\text{D}}(H) = \chi_0|H| \left[ \frac{\Delta H - \alpha(H_{\text{res}} - H)}{\Delta H^2 + (H_{\text{res}} - H)^2} \right. \\ \left. + \frac{\Delta H - \alpha(H_{\text{res}} + H)}{\Delta H^2 + (H_{\text{res}} + H)^2} \right], \quad (1)$$

where  $\alpha = 0$  if the skin depth  $\delta$  is much larger than the sample dimension perpendicular to the microwave magnetic field, and  $\alpha = 1$  if  $\delta$  is much less than this sample dimension. Here,  $\chi_0 \equiv M_0/H$  is the dimensionless volume magnetic susceptibility of the sample that can be field dependent and  $M_0$  is the thermal-equilibrium volume magnetization in the  $z$  direction in the absence of the microwave field. For the temperatures and fields of the present ESR experiments,  $\chi_0$  is independent of  $H$  [2]. In general, the parameters  $\chi_0$ ,  $\Delta H$ , and  $H_{\text{res}}$  are all temperature dependent.

The time-average microwave power  $P$  absorbed in steady state by a metallic sample containing a large concentration of local magnetic moments is [3, 6–10]

$$P(H) = F \chi''_{\text{D}}(H), \quad (2a)$$

where

$$F = \frac{\gamma H_1^2 H_{\text{res}}}{8}(A\delta), \quad (2b)$$

$A$  is the area of a surface of the sample parallel to the linearly-polarized applied microwave field  $\mathbf{H}_1$ ,  $\delta$  is the  $T$ -dependent skin depth at the microwave frequency of  $\mathbf{H}_1$  discussed in the following section, and hence  $A\delta$  is the volume of the sample beneath the surface  $A$  that is exposed to the microwave field.

Our experimental field-derivative microwave power-absorption spectra at each fixed temperature  $T$  for  $H > 0$  were fitted by the field-derivative of the Dysonian lineshape function in Eq. (1), i.e.,

$$\frac{dP}{dH} = a + b \frac{d}{dH} \left\{ H \left[ \frac{\Delta H - \alpha(H_{\text{res}} - H)}{\Delta H^2 + (H_{\text{res}} - H)^2} \right. \right. \\ \left. \left. + \frac{\Delta H - \alpha(H_{\text{res}} + H)}{\Delta H^2 + (H_{\text{res}} + H)^2} \right] \right\}, \quad (3)$$

where  $a$  is the instrumental zero-signal offset and  $b$  is the amplitude of the  $dP/dH$  spectrum. The other fitting parameters at each temperature were  $\Delta H$ ,  $\alpha$  and  $H_{\text{res}}$ . Examples of the fits are shown for crystals #2 and #3, each at  $T = 50$  K and 180 K, in Figs. 1(a) and 1(b) as solid black curves, respectively. For both crystals, the fits are very good, except for an additional feature of unknown origin in Fig. 1(b) at  $H \sim 1.2$  kOe that disappears above 70 K (see below). From Fig. 1, one also sees that the linewidth increases with increasing  $T$  for each of the two

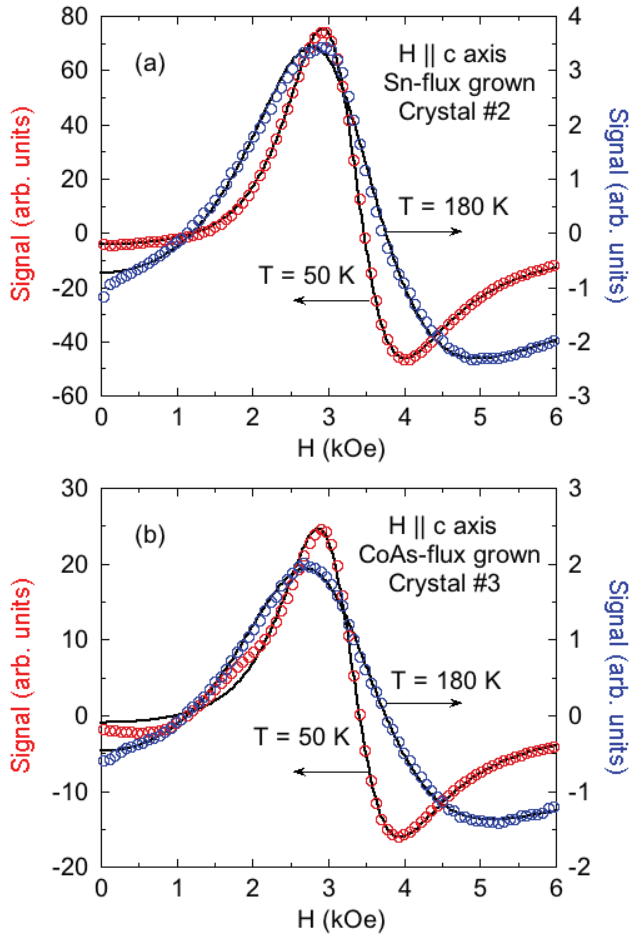


FIG. 1:  $\text{Eu}^{+2}$  field-derivative ESR spectra (open circles) at temperatures of 50 K and 180 K for (a) a Sn-flux-grown crystal #2 and (b) a CoAs self-flux-grown crystal #3 of  $\text{EuCo}_{2-y}\text{As}_2$ . The fits by Eq. (3) are shown as solid black curves.

crystals. Indeed, the resonances for the two crystals at  $T = 180$  K are cut off due to the  $H = 6$  kOe upper limit of our measurements. From the different ordinate scales for the two temperatures in each of Figs. 1(a) and 1(b), the signal amplitude strongly decreases with increasing temperature for each sample. Such a decrease is expected from the Curie-Weiss  $T$  dependence of the  $\text{Eu}^{+2} \chi_0$  [2] in Eq. (1).

### B. $\alpha$ Parameter

Shown in Fig. 2 are plots of  $\alpha$  versus  $T$  obtained from fits to the field derivative of the microwave absorption spectra such as in Fig. 1 using Eq. (3) for each of Crystals #2 and #3 both with and without the  $H$  prefactor in Eq. (1). The values obtained without the  $H$  prefactor are a factor of two to three too large compared to the correct values obtained with the  $H$  prefactor included in the fits. Furthermore, the value of  $\alpha$  must be in the range

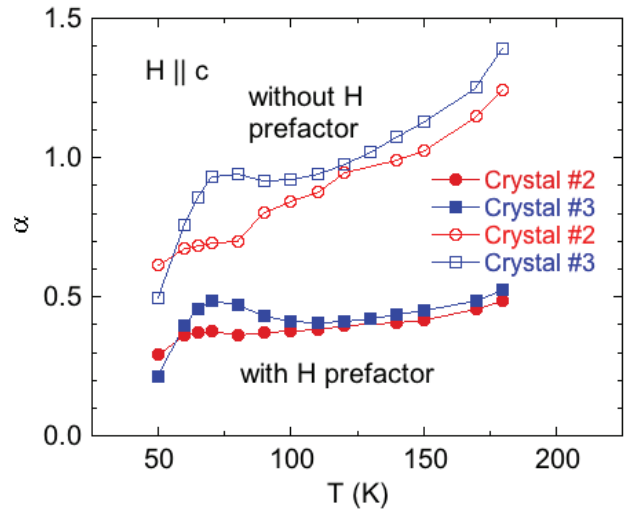


FIG. 2: Ratio  $\alpha$  of the dispersive susceptibility  $\chi'$  to the absorptive susceptibility  $\chi''$  in the Dysonian absorptive susceptibility  $\chi''_D(H)$  in Eq. (1) for Crystals #2 and #3 both with and without the  $H$  prefactor in  $\chi''_D(H)$ . All data above  $\alpha = 1$  are explicitly invalid. The correct values are the filled symbols obtained by fitting the spectra with the  $H$  prefactor.

$0 \leq \alpha \leq 1$  for a valid fit, so the values of  $\alpha > 1$  obtained without the prefactor in Fig. 2 are explicitly invalid.

The skin depth  $\delta(H, T)$  in Eq. (2b) is given in SI units by

$$\delta(H, T) = \sqrt{\frac{\rho(T)}{\pi f \mu(H, T)}}, \quad (4)$$

where  $\rho$  is the electrical resistivity,  $f$  is the microwave frequency, and  $\mu$  is the magnetic permeability of the sample. The magnetic permeability in SI units is given by

$$\mu = \mu_0[1 + (M/H)], \quad (5)$$

where  $\mu_0$  is the magnetic permeability of free space.  $M$  is the volume magnetization of the sample and in general the dimensionless ratio  $M(T, H)/H$  can be dependent on the temperature  $T$  and the magnitude and direction of the applied field  $\mathbf{H}$ . The required SI value of  $M/H$  is obtained from  $M/H$  in dimensionless cgs units via  $M/H$  (SI) =  $(4\pi)^{-1}(M/H)$  (cgs).

For  $\text{EuCo}_{2-y}\text{As}_2$  in the field and paramagnetic temperature ranges of interest in this paper,  $M/H$  in Eq. (5) is just the susceptibility  $\chi_V$  per unit volume that is given by the Curie-Weiss law in cgs units as

$$\chi_V = \frac{C/V_M}{T - \theta_p}, \quad (6a)$$

$$C \approx 9.0 \frac{\text{cm}^3 \text{ K}}{\text{mol Eu}}, \quad (6b)$$

$$\theta_p \approx 22 \text{ K}, \quad (6c)$$

$$V_M \approx 52.6 \frac{\text{cm}^3}{\text{mol Eu}}, \quad (6d)$$

where the approximate values of the molar Curie constant  $C$  and the Weiss temperature  $\theta_p$  averaged over data for five crystals and over the two field directions  $\mathbf{H} \parallel c$  and  $\mathbf{H} \parallel ab$  from Ref. [2] are given in the last three of Eqs. (6). Then Eq. (6a) gives

$$\chi_V = \frac{0.17 \text{ K}}{T - 22 \text{ K}}. \quad (7)$$

At a temperature of 50 K in the paramagnetic state where  $\chi_V$  is near its maximum value versus temperature, the value of  $\chi_V$  is

$$\chi_V(50 \text{ K}) = 0.0060 \text{ (cgs)}, \quad (8)$$

so the  $M/H$  term in Eq. (5) can be set to zero. Inserting our X-band microwave frequency  $f = 9.390 \text{ GHz}$  and the value for  $\mu_0$  into Eq. (4), one obtains

$$\delta(T)[\mu\text{m}] = 0.5194\sqrt{\rho(T)[\mu\Omega\text{cm}]} \quad (9)$$

When the static field  $\mathbf{H}$  is applied along the  $c$  axis as in this paper, the microwave magnetic field  $\mathbf{H}_1$  is parallel to the  $ab$  plane as noted above. Since the Poynting vector associated with the skin depth is normal to a surface that is perpendicular to  $\mathbf{H}$ , the microwave electric field associated with  $\mathbf{H}_1$  is also oriented in the  $ab$  plane. Hence the relevant resistivity in Eq. (9) for  $\mathbf{H} \parallel c$ -axis is the in-plane electrical resistivity  $\rho_{ab}$ , which was measured for two crystals with similar results [2] that together are approximated for the temperature range  $50 \text{ K} \leq T \leq 300 \text{ K}$  by the linear relation

$$\rho_{ab}(T) \approx 14 \text{ } \mu\Omega\text{cm} + \left( 0.083 \frac{\mu\Omega\text{cm}}{\text{K}} \right) T. \quad (10)$$

Using Eqs. (9) and (10), one obtains  $\delta = 2.2$  and  $3.2 \mu\text{m}$  at 50 K and 300 K, respectively. These values are much smaller than the  $ab$ -plane dimensions of our crystals ( $\sim \text{mm}$ ) which would therefore predict  $\alpha = 1$ . The reason we obtain  $\alpha \sim 0.4\text{--}0.5$  in Fig. 2 is unclear.

### C. Resonance Field and $g$ Factor

The resonance field  $H_{\text{res}}$  versus temperature obtained from fits of the field-derivative ESR spectra by Eq. (1) is plotted for Crystals #2 and #3 in Fig. 3(a) both with and without including the  $H$  prefactor in Eq. (1). The absence of the  $H$  prefactor gives an error of only  $\lesssim 2\%$  in the fitted  $H_{\text{res}}$  as shown. However, this error would propagate to a similar error after the demagnetizing field is corrected for as follows.

Due to the presence of highly magnetic  $\text{Eu}^{+2}$  ions with spin  $S = 7/2$ , the magnetic field  $\mathbf{H}^{\text{int}}$  internal to a sample can be significantly different from the applied field  $\mathbf{H}$ . The components of  $\mathbf{H}^{\text{int}}$  along the principal axes directions  $\beta$  are given in Gaussian cgs units by [11]

$$H_{\beta}^{\text{int}} = H_{\beta} - 4\pi N_{\text{d}\beta} M_{\beta}, \quad (11)$$

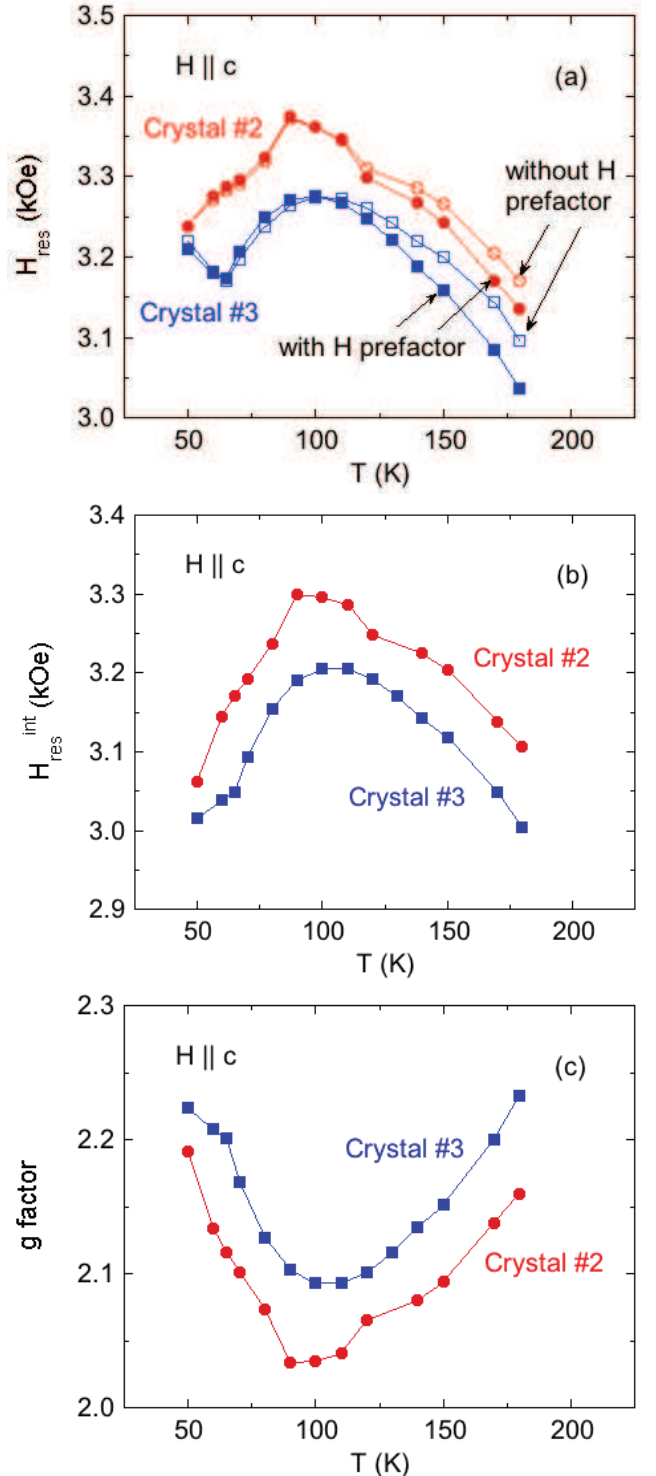


FIG. 3: (a) The measured  $\text{Eu}^{+2}$  resonance field  $H_{\text{res}}$  versus temperature  $T$  for Crystals #2 (red circles) and #3 (blue squares) of  $\text{EuCo}_{2-y}\text{As}_2$  obtained from fits of the field-derivative spectra by Eq. (3) both with (filled symbols) and without (open symbols) the  $H$  prefactor. (b) The internal resonant field  $H_{\text{res}}^{\text{int}}$  obtained from the data including the  $H$  prefactor in panel (a) after correction of the demagnetizing field according to Eq. (11). (c) The  $\text{Eu}^{+2}$   $g$ -factors for Crystals #2 and #3 versus  $T$  calculated from the data in panel (b) using Eq. (13b).

TABLE I: Dimensions and *c*-axis magnetometric demagnetization factors  $N_{dc}$  of the approximately rectangular-prism shaped Crystals #2 and #3.

Crystal	<i>ab</i> -plane (mm <sup>2</sup> )	<i>c</i> -axis (mm)	$N_{dc}$
#2 EuCo <sub>1.99(2)</sub> As <sub>2</sub> <sup>a</sup>	1.6 × 6.7	0.47	0.71
#3 EuCo <sub>1.92(4)</sub> As <sub>2</sub> <sup>b</sup>	2.5 × 4.4	0.35	0.79

<sup>a</sup>Grown in Sn flux with H<sub>2</sub>-treated Co powder

<sup>b</sup>Grown in CoAs flux with H<sub>2</sub>-treated Co powder

where the  $\beta$  principal-axis magnetization component  $M_\beta$  is in cgs units of Gauss and the magnetometric demagnetization factor  $N_{d\beta}$  is in SI units where  $0 \leq N_{d\beta} \leq 1$  and  $\sum_{\beta=1}^3 N_{d\beta} = 1$ . The dimensions and *c*-axis  $N_{dc}$  values of the crystals measured in this paper where  $\mathbf{H} \parallel c$  axis were calculated using the expression derived in Ref. [12] and are listed in Table I.

Hence at the resonance field  $H_{res}$ , Eq. (7) gives

$$M = \chi_V H_{res} = \frac{(0.17 \text{ K}) H_{res}}{T - 22 \text{ K}}. \quad (12)$$

For example, at  $T = 50$  K and taking  $N_{dc} \approx 0.75$  as in Table I, one obtains  $4\pi N_{dc} M_c = 0.19$  kOe for this term in Eq. (11), which is a large fraction of the temperature-induced change in  $H_{res}$  in Fig. 3. Thus taking the demagnetizing field into account results in a major correction to the measured  $H_{res}(T)$  for our crystals.

Shown in Fig. 3(b) are data for the internal resonant field  $H_{res}^{int}$  versus temperature obtained from the data in panel (a) for the  $H$  prefactor using Eqs. (11) and (12). One sees an unusual nonmonotonic variation of  $H_{res}^{int}$  with temperature.

The *g*-factor of the Eu<sup>+2</sup> spins is obtained from the quantum condition

$$g = \frac{hf}{\mu_B H_{res}^{int}}, \quad (13a)$$

where  $h$  is Planck's constant,  $f$  is the microwave frequency, and  $\mu_B$  is the Bohr magneton. In our experiments, the X-band microwave frequency was  $f = 9.390$  GHz. Thus one obtains

$$g = \frac{6.709}{H_{res}^{int} (\text{kOe})}. \quad (13b)$$

Plots of the *g*-factor versus  $T$  for Crystals #2 and #3 obtained from the data in Fig. 3(b) using Eq. (13b) are shown in Fig. 3(c), where the nonmonotonic variation in panel (b) is inverted. One sees *g* values enhanced above the expected  $g \approx 2$  at both low and high temperatures, with temperature-averaged values  $g_{ave} = 2.10$  and 2.15 for Crystals 2 and 3, respectively. These 5.0–7.5% enhancements above the value  $g = 2$  are consistent with the  $\approx 7.1\%$  enhancements of the Eu<sup>+2</sup> effective moment in EuCo<sub>2-y</sub>As<sub>2</sub> crystals obtained [2] from magnetic susceptibility measurements that was theoretically attributed

to spin polarization of the Co 3d-band electrons by the Eu spins [2]. This agreement indicates that the enhancement of the Eu<sup>+2</sup> effective moment arises from a conduction-electron polarization cloud that surrounds the Eu spins and that the Eu spin and polarization cloud respond as a single composite spin to an applied magnetic field in the paramagnetic state. If the polarized *d* electrons instead resided elsewhere, e.g. near the Co atoms, the observed enhanced effective moment would presumably not produce such a large enhancement of the Eu-spin *g*-factor.

#### D. Linewidth

The Lorentzian half-width of the resonance  $\Delta H$  versus  $T$  is plotted in Fig. 4(a) for Crystals #2 and #3, each both with and without the  $H$  prefactor in Eq. (3). Very little difference is observed between the values determined with or without the  $H$  prefactor in Eq. (1). The data corrected for the demagnetization field as in Fig. 3(b) are shown in Fig. 4(b). The latter data for Crystal #2 suggest possible phase transitions at  $\approx 90$  K and 120 K, whereas the data for Crystal #3 suggest a phase transition only at 65 K. Overall, the linewidth of both crystals increases with increasing temperature above 70 K as expected for relaxation of the Eu spins by exchange interactions with the conduction electrons. However the behavior is not linear in  $T$  as expected for such Korringa relaxation. The average slope between 90 K and 180 K for Crystal #2 is 8.5 Oe/K, whereas for Crystal #3 the average slope is 6.6 Oe/K. These slope values are in the range found for similar Fe-based ThCr<sub>2</sub>Si<sub>2</sub>-structure pnictide compounds containing Eu<sup>+2</sup> ions [13, 14]. The ratio  $\Delta H^{int}/H_{res}^{int}$  is plotted versus  $T$  in Fig. 4(c) for the two crystals. This ratio increases from about 0.25 at  $T \approx 60$  K to about 0.6 for  $T = 180$  K.

#### IV. SUMMARY

Excellent fits of the experimental field-derivative ESR spectra for EuCo<sub>2-y</sub>As<sub>2</sub> by the general Eq. (3) were obtained in the paramagnetic phase at temperatures from 50 K to 180 K for Crystals #2 and #3. This equation, as discussed in Ref. [3], contains a theoretically-required magnetic-field ( $H$ ) prefactor not utilized previously to our knowledge when fitting such ESR spectra. We tested the influence of this  $H$  prefactor on the parameters obtained from the fits of the ESR spectra for EuCo<sub>2-y</sub>As<sub>2</sub>. We find that whether or not this prefactor is included in the fit function gives only a few percent difference at most in the fitted values of  $\Delta H$  and  $H_{res}$ , but the fitted value of  $\alpha$  without the  $H$  prefactor is up to a factor of three too large compared to the values obtained when the prefactor is included in the fit function. Furthermore, some of the fitted  $\alpha$  values obtained in the absence of the  $H$  prefactor exceed the physical upper limit of unity for  $\alpha$ .

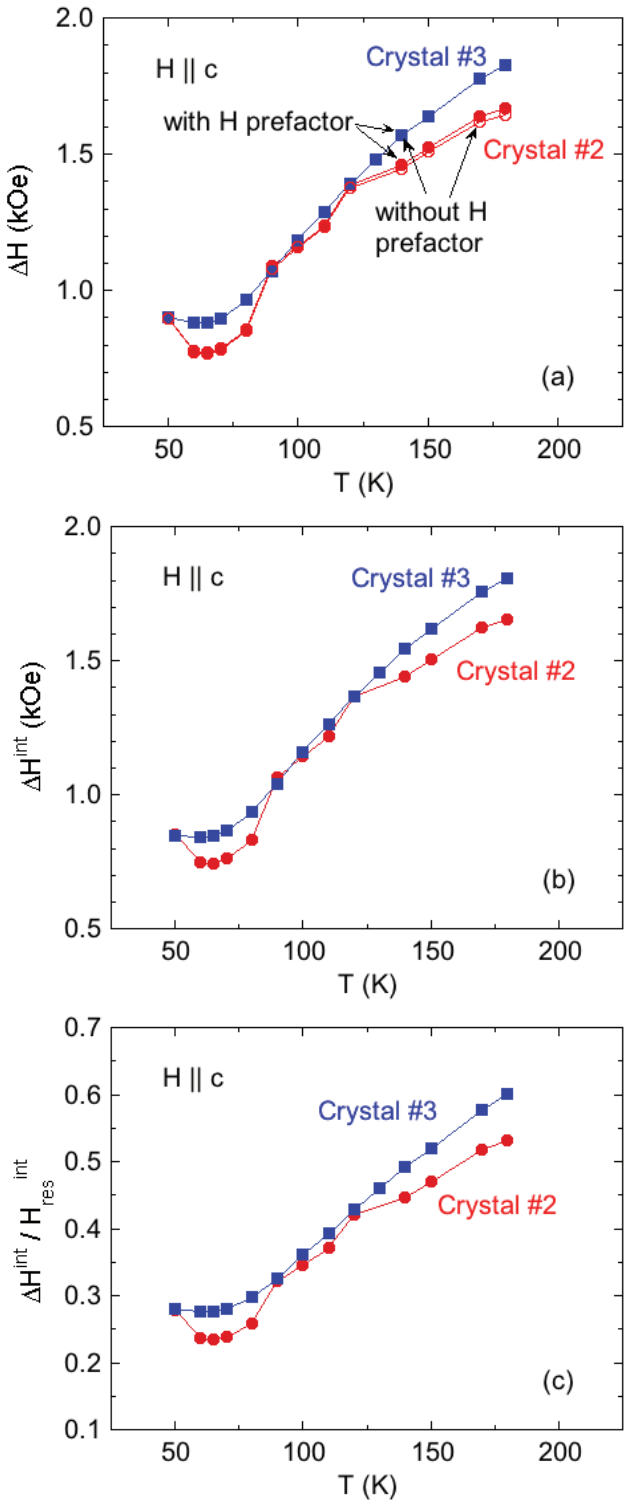


FIG. 4: (a) Lorentzian half-width  $\Delta H$  versus temperature  $T$  for Crystals #2 and #3 obtained by fitting the field-derivative ESR spectra by Eq. (3) both with and without the  $H$  prefactor in Eq. (3) as indicated. (b) Half-width  $\Delta H^{\text{int}}$  corrected for the demagnetization field versus  $T$  as in Fig. 3(b) for  $H^{\text{int}}$ . (c) The ratio  $\Delta H^{\text{int}}/H_{\text{res}}$  versus  $T$ .

With the  $H$  prefactor included in the fit, the  $\alpha$  parameter was found to be nearly independent of temperature above 70 K with a value of  $\approx 0.5$ . According to our analysis of the skin depth in comparison to the dimension of the sample surface perpendicular to the  $c$  axis ( $\sim$  mm), the expected value of  $\alpha$  is 1 according to Dyson's theory. This discrepancy remains to be resolved.

The temperature-dependent resonant field and  $g$ -factor for Crystal #3 showed evidence for some type of phase transition at 65 K, whereas the data for Crystal #2 suggested possible transitions at 90 K and 120 K. Additional experiments are required to determine whether these features are associated with phase transitions.

The Lorentzian resonance half-width  $\Delta H$  increases monotonically, but nonlinearly, from 60 K to 180 K with an average slope of 8.5 and 6.6 Oe/K for Crystals #2 and #3, respectively. These values are in the range found for similar ThCr<sub>2</sub>Si<sub>2</sub>-structure  $\text{Eu}M_2X_2$  compounds, where  $M = \text{Fe}$  and/or mixtures with other transition metals and  $X$  is As and/or mixtures with P.

We obtained microscopic information on the enhancement of the Eu moment that was reported from magnetic susceptibility measurements [2], which was the main goal of the present work. The  $g$ -factor obtained from the internal resonant field is found to vary nonmonotonically with temperature. For example, for Crystal #3 we find a minimum  $g = 2.09$  at  $\approx 100$  K and maximum values of  $\approx 2.23$  at our lower and upper temperature limits of 50 K and 180 K, respectively. That the  $g$ -factor may be temperature dependent in the paramagnetic state was previously inferred in Ref. [2]. The temperature-averaged  $g$  values for the two crystals are 2.10 and 2.15, respectively. This 5–7.5% enhancement above  $g = 2$  is consistent with the 7% enhancement of the effective moment of the Eu spins found [2] from magnetic susceptibility measurements in the paramagnetic state. The *ab initio* electronic structure calculations [2] indicated that the enhancement of the Eu moments originates from ferromagnetic polarization of the Co 3d conduction electrons by the Eu spins. The present work indicates that this electron polarization is physically located around the Eu spins, and hence that the polarized  $d$  electrons form a composite enhanced spin with each Eu spin. On the other hand, the saturation moments at  $H = 140$  kOe obtained for crystals from the same growth batches #2 and #3 were  $\mu_{\text{sat}} = 7.04$  and  $7.56 \mu_{\text{B}}/\text{Eu}$ , respectively, where the first value is hardly enhanced and the second one is enhanced above the value expected for  $g = 2$  by 8.0%. The reason there was little enhancement of  $\mu_{\text{sat}}$  of the crystal from batch #2 whereas the effective moment of this crystal was enhanced by 8.6% according to Tables III and IV in Ref. [2] is unclear.

A similar but opposite dichotomy to that seen for  $\text{EuCo}_{2-y}\text{As}_2$  growth batch #2 was observed for Gd metal containing  $\text{Gd}^{+3}$  spins-7/2. Whereas the low- $T$  saturation moment is enhanced from 7.00 to 7.55  $\mu_{\text{B}}/\text{Gd}$ , the effective moment obtained from the magnetic susceptibility in the paramagnetic state above the ferromagnetic

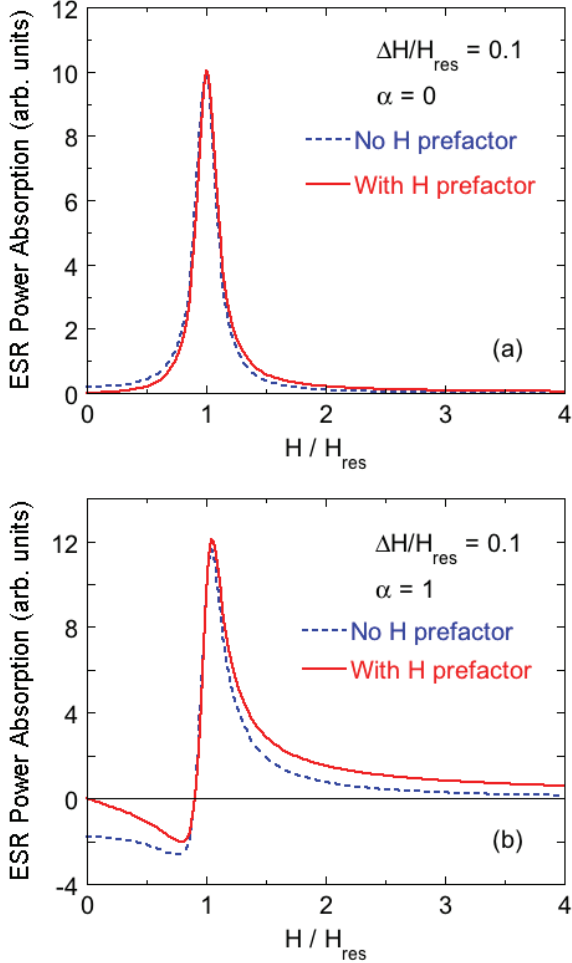


FIG. 5: ESR power absorption spectra with reduced Lorentzian half-width  $\Delta H/H_{\text{res}} = 0.1$  versus the reduced applied field  $H/H_{\text{res}}$  for  $\alpha$  values of (a) 0 and (b) 1, both without and with the  $H$  prefactor in Eq. (1) in the main text.

Curie temperature  $T_C = 294$  K [15] is  $7.98(5)$   $\mu_B/\text{Gd}$  [16], which is the same within the errors as predicted for  $g = 2$ . In two separate studies, ESR measurements of Gd in the paramagnetic state also yielded unenhanced  $g$ -factor values of  $1.95(3)$  and  $1.97$ , respectively [17, 18]. It is peculiar that the low- $T$ , high- $H$  saturation moment in Gd metal is strongly enhanced whereas the paramagnetic effective moment and  $g$ -factor at temperatures above  $T_C$  are not.

#### Appendix: Field-Integrated ESR Intensity

It is common in ESR studies of local moments in metals to ignore the  $H$  prefactor in the power absorption spectrum in Eq. (1). Then irrespective of the (positive) values of  $\alpha$ ,  $H_{\text{res}}$  and  $\Delta H$ , the integral of the absorbed power over all  $H$  at a given temperature  $T$  obtained from

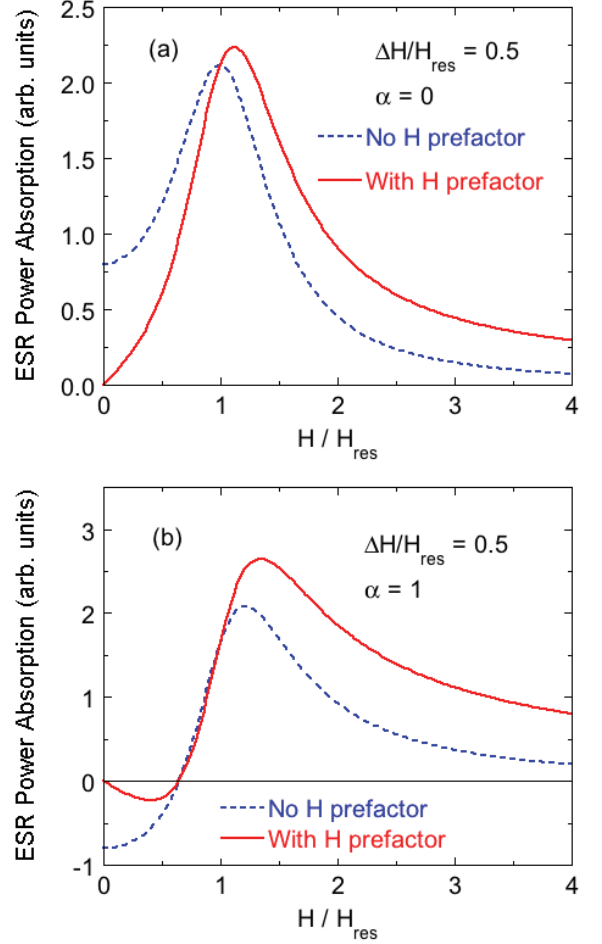


FIG. 6: Same as Fig. 5 except that  $\Delta H/H_{\text{res}} = 0.5$ .

Eqs. (1) and (2a) is

$$\int_0^\infty P(H, T) dH \propto \chi_0(T) \quad (H \text{ prefactor absent}). \quad (\text{A.1})$$

Therefore one can compare the  $T$  dependence of the integral with  $\chi_0(T)$  measured with a dc magnetometer. For  $\Delta H/H_{\text{res}} \ll 1$  this procedure is accurate and useful. However, we have found that major differences between the two measures of  $\chi_0(T)$  can occur when broad lines with  $\Delta H/H_{\text{res}} \sim 1$  are observed such as in our ESR study of  $\text{EuCo}_{2-y}\text{As}_2$  described in the main text.

Before further discussing the field-integrated absorbed power, we first plot the ESR power absorption spectrum versus reduced field  $H/H_{\text{res}}$  because the shape of such spectra for  $\alpha > 0$  is perhaps unexpected. Shown in Fig. 5(a) is the conventional Lorentzian lineshape for a relatively narrow spectrum with  $\Delta H/H_{\text{res}} = 0.1$  with and without the  $H$  prefactor in Eq. (1), where the presence or absence of the  $H$  prefactor is seen to make a relatively small difference. On the other hand, when  $\alpha$  takes its maximum value  $\alpha = 1$ , a qualitative difference in the lineshape occurs where now there is also a significant difference when the theoretically-required  $H$  pref-

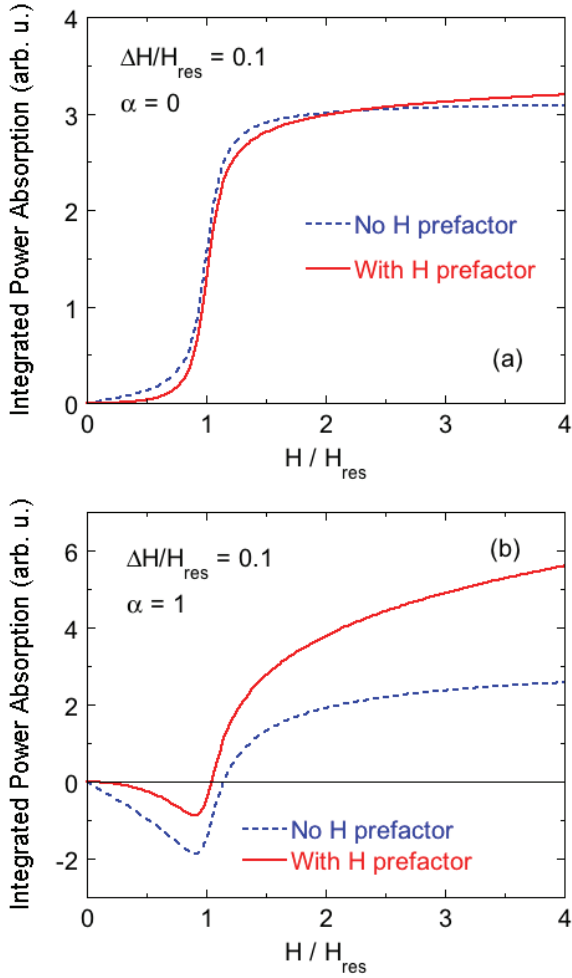


FIG. 7: Field-integrated ESR power absorption spectra obtained from Eq. (A.2) with reduced Lorentzian half-width  $\Delta H/H_{\text{res}} = 0.1$  versus the reduced applied field  $H/H_{\text{res}}$  for  $\alpha$  values of (a) 0 and (b) 1. If the  $H$  prefactor in Eq. (1) is ignored, the integrated power is  $\lim_{H \rightarrow \infty} = \pi\chi_0$  for  $\alpha = 0$  and 1, whereas with the prefactor present one obtains  $\lim_{H \rightarrow \infty} = \infty$  for either  $\alpha$  value.

actor is ignored as shown in Fig. 5(b). For applied fields  $H/H_{\text{res}} \lesssim 1$  and  $\alpha = 1$ , the ESR power absorbed is negative, which means that the sample is transferring energy from the temperature reservoir with which it is in thermal contact to the source of the microwave power.

Shown in Fig. 6(a) and 6(b) are data as in Fig. 5 except that now the reduced linewidth is increased to  $\Delta H/H_{\text{res}} = 0.5$  as was approximately obtained in our experiments on  $\text{EuCo}_{2-y}\text{As}_2$ . Here the difference in the absorption spectra between the cases with and without the  $H$  prefactor is much more pronounced.

The field-dependent integral of the absorbed power at a given temperature  $T$  is defined as

$$P_{\text{int}}(H) \propto \int_0^H \chi''(H') dH'. \quad (\text{A.2})$$

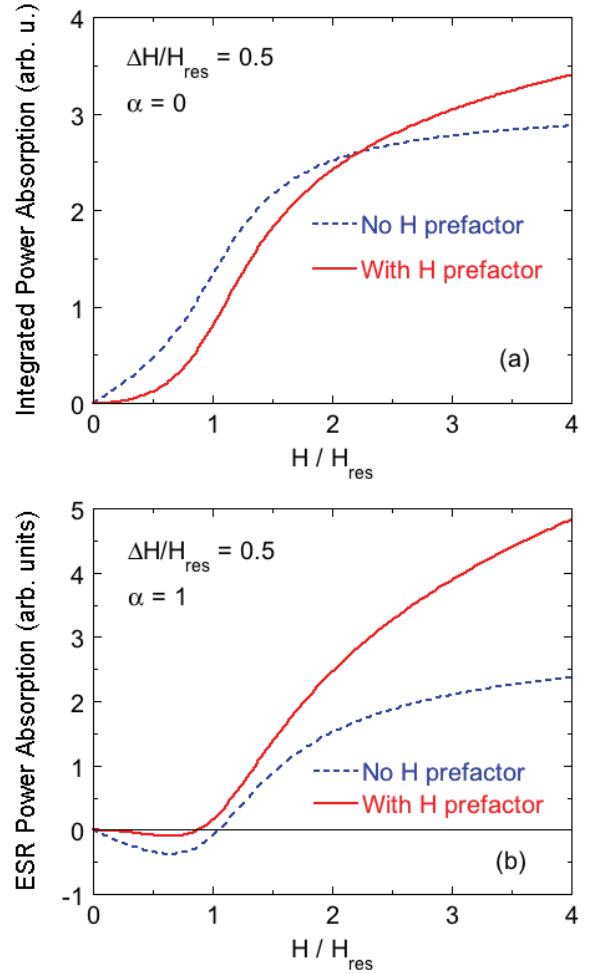


FIG. 8: Same as Fig. 7 except that  $\Delta H/H_{\text{res}} = 0.5$ .

If the  $H$  prefactor in Eq. (1) is not present one obtains

$$\int_0^\infty \chi''(H') dH' = \pi\chi_0 \quad (\text{no } H \text{ prefactor}). \quad (\text{A.3})$$

On the other hand when the  $H$  prefactor is included as required by theory one has

$$\int_0^\infty \chi''(H') dH' = \infty \quad (\text{with } H \text{ prefactor}). \quad (\text{A.4})$$

This (logarithmic) divergence occurs because for large  $H$ ,  $\chi''(H)$  becomes

$$\chi''(H/H_{\text{res}} \gg 1) = \frac{2(\alpha + \Delta H/H_{\text{res}})}{H/H_{\text{res}}}. \quad (\text{A.5})$$

Plots of  $P_{\text{int}}(H/H_{\text{res}})$  in Eq. (A.2) with  $\Delta H/H_{\text{res}} = 0.1$  for  $\alpha = 0$  and 1 are shown in Fig. 7. One sees that for  $\alpha = 0$  there is relatively little difference between the curves calculated with and without the  $H$  prefactor in Eq. (1) for  $H/H_{\text{res}} \leq 4$ . However, for  $\alpha = 1$  a major difference exists between the two curves. When the linewidth increases to

$\Delta H/H_{\text{res}} = 0.5$ , the discrepancy between the integrated power absorption with and without the  $H$  prefactor for each of the two  $\alpha$  values is large as shown in Fig. 8.

Materials Sciences and Engineering. Ames Laboratory is operated for the U.S. Department of Energy by Iowa State University under Contract No. DE-AC02-07CH11358.

### Acknowledgments

This research was supported by the U.S. Department of Energy, Office of Basic Energy Sciences, Division of Ma-

---

[1] N. S. Sangeetha, E. Cuervo-Reyes, A. Pandey, and D. C. Johnston, EuCo<sub>2</sub>P<sub>2</sub>: A model molecular-field helical Heisenberg antiferromagnet, *Phys. Rev. B* **94**, 014422 (2016).

[2] N. S. Sangeetha, V. K. Anand, Eduardo Cuervo-Reyes, V. Smetana, A.-V. Mudring, and D. C. Johnston, Enhanced moments of Eu in single crystals of the metallic helical antiferromagnet EuCo<sub>2-y</sub>As<sub>2</sub>, *Phys. Rev. B* **97**, 144403 (2018).

[3] D. C. Johnston, Dysonian Electron-Spin-Resonance Spectra of Local Magnetic Moments in Metals, *arXiv*: 1808.05436.

[4] V. A. Ivanshin, J. Deisenhofer, H.-A. Krug von Nidda, A. Loidl, A. A. Mukhin, A. M. Balbashov, and M. V. Eremin, ESR study in lightly doped La<sub>1-x</sub>Sr<sub>x</sub>MnO<sub>3</sub>, *Phys. Rev. B* **61**, 6213 (2000).

[5] J. P. Joshi and S. V. Bhat, On the analysis of broad Dysonian electron paramagnetic resonance spectra, *J. Magn. Res.* **168**, 284 (2004). In this paper,  $\Delta H$  is the full width at half maximum Lorentzian peak height instead of the half-width at half maximum used in the present paper and in Ref. [4].

[6] A. Abragam, *Principles of Nuclear Magnetism* (Clarendon, Oxford, 1961).

[7] C. P. Slichter, *Principles of Magnetic Resonance* (Harper & Row, New York, 1963).

[8] G. E. Pake and T. L. Estle, *The Physical Principles of Electron Paramagnetic Resonance*, 2<sup>nd</sup> edition (Benjamin, Reading, MA, 1973).

[9] C. P. Poole, Jr., *Electron Spin Resonance*, 2<sup>nd</sup> edition (Wiley, New York, 1983).

[10] G. Feher and A. F. Kip, Electron Spin Resonance Absorption in Metals. I. Experimental, *Phys. Rev.* **98**, 337 (1955).

[11] D. C. Johnston, Magnetic dipole interactions in crystals, *Phys. Rev. B* **93**, 014421 (2016).

[12] A. Aharoni, Demagnetizing factors for rectangular ferromagnetic prisms, *J. Appl. Phys.* **83**, 3432 (1998).

[13] J. J. Ying, T. Wu, Q. J. Zheng, Y. He, G. Wu, Q. J. Li, Y. J. Yan, Y. L. Xie, R. H. Liu, X. F. Wang, and X. H. Chen, Electron spin resonance in EuFe<sub>2-x</sub>Co<sub>x</sub>As<sub>2</sub> single crystals, *Phys. Rev. B* **81**, 052503 (2010).

[14] H.-A. Krug von Nidda, S. Kraus, S. Schaile, E. Denger, N. Pascher, M. Hemmida, M. J. Eom, J. S. Kim, H. S. Jeevan, P. Gegenwart, J. Deisenhofer, and A. Loidl, Electron spin resonance in Eu-based iron pnictides, *Phys. Rev. B* **86**, 094411 (2012).

[15] S. Yu. Dan'kov, A. M. Tishin, V. K. Pecharsky, and K. A. Gschneidner, Jr., Magnetic phase transitions and the magnetothermal properties of gadolinium, *Phys. Rev. B* **57**, 3478 (1998).

[16] H. E. Nigh, S. Legvold, and F. H. Spedding, Magnetization and Electrical Resistivity of Gadolinium Single Crystals, *Phys. Rev.* **132**, 1092 (1963).

[17] A. F. Kip, C. Kittel, A. M. Portis, R. Barton, and F. H. Spedding, Microwave Resonance Absorption in Gadolinium Metal, *Phys. Rev.* **89**, 518 (1953).

[18] Y. Chiba and A. Nakamura, E. S. R. Study on Gadolinium Metal, *J. Phys. Soc. Jpn.* **29**, 792 (1970).